Effect of strain on the magnetoexciton ground state in InP/$Ga_xIn_{1-x}P$ quantum disks

K. L. Janssens,* B. Partoens,† and F. M. Peeters‡
Departement Natuurkunde, Universiteit Antwerpen (UIA), Universiteitsplein 1, B-2610 Antwerpen, Belgium
(Received 2 December 2002; published 26 June 2003)

The ground-state properties of an exciton in a self-assembled quantum disk are calculated in the presence of a perpendicular magnetic field. For sufficient wide and thin dots, the strain field leads to a confinement of the heavy hole within the dot and the system is type I, while the light hole is confined outside the dot and the system is type II. However, with increasing disk thickness, the strain induces a transition of the heavy hole from inside the disk towards the radial boundary outside the disk. For the exciton, we predict a heavy-hole to light-hole transition as a function of the disk thickness, i.e., forming a ''ringlike'' hole wave function. There is a range of parameters (radius and height of the disk) for which a magnetic field can induce such a heavy-to-light hole transition. The diamagnetic shift was compared with results from magnetophotoluminescence experiments, where we found an appreciable discrepancy. The origin of this discrepancy was investigated by varying the disk parameters, the valence-band offset, and the effective masses.

DOI: 10.1103/PhysRevB.67.235325 PACS number(s): 73.21.La, 71.35.Ji, 85.35.Be

I. INTRODUCTION

Quantum dots have been the subject of intensive studies during the past two decades, because of their zero-dimensional nature with the corresponding δ-function-like density of states.[1] Arakawa and Sakaki[2] reported in 1982 a theoretical prediction of promising advantages, such as a low and temperature-independent threshold current, of quantum dot lasers compared to the conventional quantum well semiconductor laser.

The use of the Stranski-Krastanow growth mode to fabricate so-called ''self-assembled'' quantum dots meant a breakthrough in the further research of semiconductor dots. The fast and easy nature of this growth process, together with the possibility to fabricate small and defect-free dots, had a great advantage over previous types of dots, as, e.g., colloidal dots or dots created by lithographic techniques. The formation of self-assembled dots requires two semiconductor materials with a substantially different lattice parmeter, which are grown on top of each other. Such lattice-mismatched heteroepitaxy gives rise to the formation of nanometer sized islands, governed by strain-relaxation effects.

Confinement of charge carriers in quantum dots occurs because of the difference in bandstructure of the two semiconductor materials. One can define two types of quantum dots, namely, type-I and type-II, depending on the band alignments. In the case of type-I dots, both the electron and the hole are confined inside the dot. For type-II dots, the confinement inside the dot occurs only for one of the charge carriers, i.e., electron or hole, whereas the dot forms an antidot for the other particle. Examples of type-II dots are the InP/$Ga_xIn_{1-x}P$ (Refs. 3 and 4) or InP/GaAs dots with the electron confined in the dot, and the hole in the barrier, and the GaSb/GaAs (Ref. 5) or InAs/Si (Ref. 6) dots where the hole is located inside the dot, but the electron remains in the barrier.

Up to now most research was devoted to type-I structures,[7–13] while type-II dots have attracted fewer attention. Theoretical studies considering InP/$Ga_xIn_{1-x}P$ dots were performed by Pryor *et al.*[14] and Tadić *et al.*[15] where a strain-dependent $\mathbf{k}\cdot\mathbf{p}$ Hamiltonian was used to calculate the electronic structure. GaSb/GaAs quantum dots were investigated by Lelong *et al.*[16] who studied excitons and charged excitons, and by Kalameitsev *et al.*[17] who investigated the effect of a magnetic field. In previous work we relied on a simplified effective-mass approximation, without considering the effect of strain, to study single and coupled type-II dots in the presence of external magnetic[18] and electric[19] fields.

The formation of self-assembled quantum dots is inextricably bound up with the occurrence of strain fields in and around the dots. The strain will have a large impact on the band structure, and hereby also on the optical properties of the dots. The hydrostatic component of the strain will shift the conduction- and valence-band edges, while the biaxial strain modifies the valence bands by splitting the degeneracy of the light- and heavy-hole bands.

Different theoretical models exist to obtain the strain distribution in and around self-assembled quantum dots. Well-known and extensively used are the continuum mechanical (CM) model[9,15] and the valence force field (VFF) model.[9,20,21] In the CM model, the elastic energy is minimized to obtain the distribution of the displacement in the structure and the corresponding strain fields, whereas the VFF model is an atomistic approach, which uses phenomenological expressions for the elastic energy, depending on the atomic coordinates. Pryor *et al.*[14] compared the two methods and found agreement for small strains, whereas for larger strains discrepancies were reported.[22] This was corroborated very recently by Tadić *et al.*,[15] who also compared both methods for cylindrical InAs/GaAs and InP/$In_{1-x}Ga_xP$ dots, and found a better agreement for InP/$Ga_xIn_{1-x}P$ than for InAs/GaAs dots, where the latter has the largest lattice mismatch.

A more simple method to calculate the strain fields near an isotropic quantum dot was presented by Downes *et al.*,[23] who used Eshelby's theory of inclusions[24] to express the strain distribution in quantum dot structures. This approach was adapted by Davies, who showed that the elastic field can be derived from a scalar potential that obeys a Poisson equation with the lattice mismatch as charge density.[25]

In the present paper, we follow the work of Davies[25] and use the so-called isotropic elasticity model to calculate the strain fields around a single cylindrical quantum disk. The results for this structure have recently been shown to be in good agreement with results obtained by the CM model.[15,21] The strain distribution is used as an input to calculate the modification to the band structure. We use a single-band effective-mass approximation to calculate the exciton properties in InP/$Ga_xIn_{1-x}P$ quantum disks in the presence of a perpendicular magnetic field, considering both heavy- and light-hole bands. The three-dimensional confinement is known to cause drastic effects on the band structure close to the zone center, inducing a mixing of the valence bands. However, strain causes a splitting of the heavy- and light-hole bands, therefore reducing the mixing and making the single-band effective-mass approach a justifiable first approximation.[26]

The eight-band $\mathbf{k}\cdot\mathbf{p}$ theory and consequently also the more simplified two-band effective-mass model are most accurate in the vicinity of the Γ point. However, the accuracy of the eight-band $\mathbf{k}\cdot\mathbf{p}$ model decreases for smaller dots and more elaborate methods, as empirical pseudopotential (EP) calculations are necessary. Comparison for InAs/GaAs quantum dots shows a reasonable agreement between eight-band $\mathbf{k}\cdot\mathbf{p}$ and EP calculations for dot base lengths $b \geqslant 9$ nm.[27] The contributions of "large-$|\mathbf{k}|$" states are in this size range found to be negligible. As the dots in the present study have a diameter ≈ 15 nm, we therefore neglect states originating from larger $\mathbf{k}$ values.

The paper is organized as follows. In Sec. II, we explain our theoretical model. Section III discusses the strain induced type-I to type-II transition for the heavy hole, while Sec. IV is dedicated to the heavy-hole to light-hole transition of the ground state. In Sec. V, we compare our numerical results with experimental results of Ref. 3. Our results are summarized in Sec. VI.

II. THEORETICAL MODEL

The strain was calculated by adapting the method used in Ref. 25, and which was already described in Ref. 15. The elements of the strain tensor are given by

$$\varepsilon_{ij}(\mathbf{r}) = \varepsilon_0 \delta_{ij} - \frac{\varepsilon_0}{4\pi}\frac{1+\nu}{1-\nu}\oint_{S'}\frac{(r_i - r_i')dS_j'}{|\mathbf{r}-\mathbf{r}'|^3}, \tag{1}$$

where ε_0 is the lattice mismatch between InP and $Ga_xIn_{1-x}P$, given by $\varepsilon_0 = (a_{\mathrm{InP}} - a_{\mathrm{GaInP}})/a_{\mathrm{GaInP}}$. Furthermore, ν denotes the Poisson ratio, generally chosen to be 1/3 for zinc-blende-type semiconductors, S' is the surface of the dot, and i runs over x, y, and z.

For the calculation of the exciton properties, we used a mean-field-type approach, which is equivalent, for this problem, to the Hartree-Fock approximation. This approach was previously introduced by us for type-II quantum dots where strain[18,28] was neglected. The coupled single-particle equations are given by

$$\left[H_{e(h)} - \frac{e^2}{4\pi\epsilon}\int \frac{\rho_{h(e)}(r',z')}{|\mathbf{r}-\mathbf{r}'|}d\mathbf{r}'\right]\psi_{e(h)}(r_{e(h)},z_{e(h)}) = \epsilon_{e(h)}\psi_{e(h)}(r_{e(h)},z_{e(h)}), \tag{2}$$

with H_e (H_h) the single-particle Hamiltonian for the electron (hole). In the presence of strain, the single-particle Hamiltonian for the electron can be written as

$$H_e = -\frac{\hbar^2}{2}\nabla\frac{1}{m^*(\mathbf{r})}\nabla + V_c(\mathbf{r}) + a_c\varepsilon_{hy}(\mathbf{r}) + \frac{\hbar^2}{2m^*(\mathbf{r})}\frac{l_e^2}{r^2} + \frac{l_e}{2}\hbar\omega_{c,e} + \frac{1}{8}m^*(\mathbf{r})\omega_{c,e}^2 r^2, \tag{3}$$

with $\omega_{c,e}(\mathbf{r}) = eB/m^*(\mathbf{r})$, where $m^*(\mathbf{r})$ is the position-dependent electron effective mass, a_c is the conduction-band deformation potential, l_e is the electron angular momentum, and the hydrostatic strain ε_{hy} is defined by $\varepsilon_{xx}+\varepsilon_{yy}+\varepsilon_{zz}$.

Furthermore, we make a distinction between the heavy and the light hole, as the strain will act differently on them. For the heavy hole, we have

$$H_{hh}(\mathbf{r}) = \frac{\hbar^2}{2}\left\{\nabla_\parallel\frac{1}{m_{hh,\parallel}(\mathbf{r})}\nabla_\parallel + \nabla_z\frac{1}{m_{hh,z}(\mathbf{r})}\nabla_z\right\} + V_h(\mathbf{r}) + a_v\varepsilon_{hy}(\mathbf{r}) + b[(\varepsilon_{xx}+\varepsilon_{yy})/2 + \varepsilon_{zz}] + \frac{\hbar^2}{2m_{hh,\parallel}(\mathbf{r})}\frac{l_h^2}{r^2} - \frac{l_h}{2}\hbar\omega_{c,hh} + \frac{1}{8}m_{hh,\parallel}(\mathbf{r})\omega_{c,hh}^2 r^2, \tag{4}$$

with $\omega_{c,hh}(\mathbf{r}) = eB/m_{hh,\parallel}(\mathbf{r})$, and $m_{hh,\parallel}^{-1}(\mathbf{r}) = [\gamma_1(\mathbf{r}) + \gamma_2(\mathbf{r})]$ the in-plane heavy-hole effective mass, $m_{hh,z}^{-1}(\mathbf{r}) = [\gamma_1(\mathbf{r}) - 2\gamma_2(\mathbf{r})]$ the heavy-hole effective mass along the z direction. The valence-band deformation potentials are given by a_v and b, and $\gamma_i(\mathbf{r})$ are the Luttinger parameters.

For the light hole, this becomes

$$H_{lh}(\mathbf{r}) = \frac{\hbar^2}{2m_0}\left\{\nabla_\parallel\frac{1}{m_{lh,\parallel}(\mathbf{r})}\nabla_\parallel + \nabla_z\frac{1}{m_{lh,z}(\mathbf{r})}\nabla_z\right\} + V_h(\mathbf{r}) + a_v\varepsilon_{hy}(\mathbf{r}) - b[(\varepsilon_{xx}+\varepsilon_{yy})/2 + \varepsilon_{zz}] + \frac{\hbar^2}{2m_{lh,\parallel}(\mathbf{r})}\frac{l_h^2}{r^2} - \frac{l_h}{2}\hbar\omega_{c,lh} + \frac{1}{8}m_{lh,\parallel}(\mathbf{r})\omega_{c,lh}^2 r^2, \tag{5}$$

with $\omega_{c,lh}(\mathbf{r}) = eB/m_{lh,\parallel}(\mathbf{r})$, and $m_{lh,\parallel}^{-1}(\mathbf{r}) = [\gamma_1(\mathbf{r}) - \gamma_2(\mathbf{r})]$ the in-plane light-hole effective mass, and $m_{lh,z}^{-1}(\mathbf{r}) = [\gamma_1(\mathbf{r}) + 2\gamma_2(\mathbf{r})]$ the light-hole effective mass along the z direction.

We solved the coupled single-particle equations self-consistently using an iterative procedure. More information about the implementation and numerical procedure can be found in Ref. 28. After convergence of the iteration procedure, the total energy is given by

TABLE I. Material parameters, taken from Ref. 15.

Parameter	InP	$Ga_{0.51}In_{0.49}P$
$m_e^*(m_0)$	0.077	0.125
γ_1	4.95	5.24
γ_2	1.65	1.53
$m_{hh,\parallel}$	0.1515	0.1477
$m_{hh,z}$	0.606	0.4587
$m_{lh,\parallel}$	0.303	0.269
$m_{lh,z}$	0.121	0.1205
E_g (eV)	1.424	1.97
V_c (eV)	1.379	1.97
V_v (eV)	−0.045	0.0
a_c (eV)	−7.0	
a_v (eV)	0.4	
b (eV)	−2.0	
ϵ	12.61	12.61
a (nm)	0.58687	0.56532

$$E_{exciton}=E_e+E_h+\frac{e^2}{4\pi\epsilon}\int\int\frac{\rho_e(r,z)\rho_h(r',z')}{|\mathbf{r}-\mathbf{r}'|}d\mathbf{r}d\mathbf{r}', \tag{6}$$

where E_e and E_h are the single-particle energies.

For our numerical calculation, we took the material parameters of $InP/Ga_xIn_{1-x}P$, as used in Refs. 14 and 15, which are given in Table I. Here $m_{hh,\parallel}$, $m_{hh,z}$, $m_{lh,\parallel}$, and $m_{lh,z}$ are calculated from the Luttinger parameters using the formulas mentioned above. From Table I, it follows that the valence-band offset for this system is *negative* ($V_h=-45$ meV), i.e., we have a type-II system. This appeared to be rather controversial, however, as a theoretical calculation based on first principles by Wei and Zunger[29] showed that the band offset should be positive ($V_h=55$ meV), leading to a type-I confinement. Experimentally, Hayne *et al.*[3,4] conclude that the hole should be located in the barrier, and that the system is type II. In a first step, we will use the negative band offset, as we used previously. Later, we will investigate how our results are modified when we take the positive bulk hole band offset.

III. STRAIN INDUCED TYPE-I TO TYPE-II TRANSITION FOR THE HEAVY HOLE

As follows from the equations, hydrostatic strain shifts the conduction- and valence-band offsets. Furthermore, the biaxial strain induces a splitting of the heavy- and light-hole bands. The heavy-hole band is shifted towards higher energies, whereas the light-hole band shifts towards lower energies.

The unstrained valence-band offset is slightly negative, i.e., $V_h=-45$ meV, but the heavy-hole band offset will become strongly positive after strain is introduced. The heavy hole will thus be strongly confined inside the disk, making the system type I. In contrast, the light-hole band decreases in energy, making the system even more type II and the light hole will be located outside the disk. The numerical results

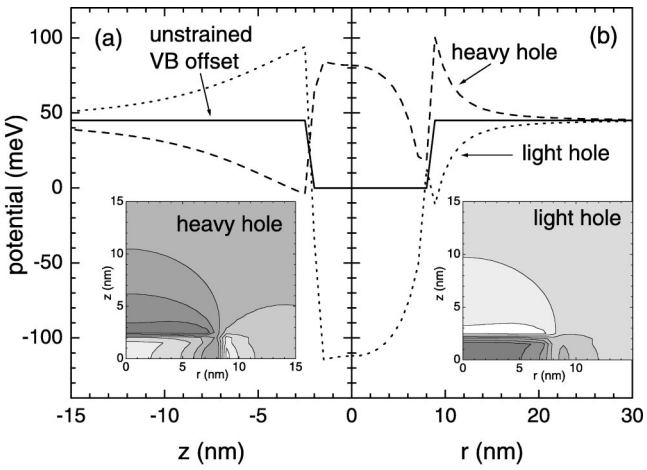

FIG. 1. The confinement potentials for the hole along the z direction (a) and along the radial direction (b) for a disk with radius $R=8$ nm and thickness $d=4$ nm. The unstrained valence-band offset is shown by the solid curve, whereas the dashed and dotted curves denote, respectively, the heavy- and light-hole confinement potentials. The insets show contour plots of the heavy- (left panel) and light- (right panel) hole confinement potentials. The white regions denote the highest potential, where the respective hole will be located.

for a disk of radius $R=8$ nm and thickness $d=4$ nm are shown in Fig. 1. The unstrained valence-band offset (solid curve) is depicted together with the strained heavy-hole (dashed curve) and light-hole (dotted curve) band offsets, in the direction perpendicular to the disk along its center [Fig. 1(a)] and along its radial [Fig. 1(b)]. Contour plots of the heavy- and light-hole potentials are depicted as insets in Fig. 1. For the heavy hole, we find a deep potential maximum in the middle of the quantum disk. Notice that in the radial direction, this potential decreases towards the disk boundary and increases again just after the radial disk boundary and can have even a higher maximum, but which in the considered case is narrower. The light-hole potential shows the deepest confinement (i.e., highest potential) in the barrier material, just on top and below the disk, which will be the preferential position for the light hole.

We found that when we increased the thickness d of the disk, the heavy hole moves towards the radial boundary of the disk. This effect is purely due to the strain, which increases the potential maximum at the radial boundary with respect to the potential inside the disk [see Fig. 2(b)]. For thicker disks, the height of the potential *in* the disk systematically decreases, making it eventually preferable for the heavy hole to move out of the disk and the system becomes type II also for the heavy hole. Figure 2(a) depicts the downward shift of the confinement potential for increased d along the z direction. We summarized our results in the phase diagram in Fig. 3. To construct this figure, we calculated the probability of the heavy hole to sit at the radial boundary of the disk,

$$P_{side}=2\pi\int_{-\infty}^{\infty}dz_h\int_R^{\infty}dr_h\ r_h|\Psi_{hh}(r_h,z_h)|^2. \tag{7}$$

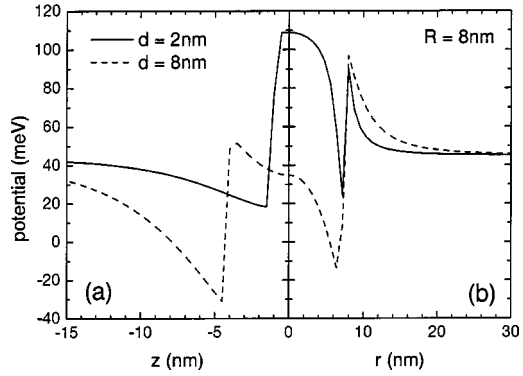

FIG. 2. Heavy-hole confinement potentials along the radial (a) and z (b) directions, for a disk with radius $R=8$ nm and thickness $d=2$ nm (solid curve) and $d=8$ nm (dashed curve).

The line in Fig. 3 indicates the probability $P_{side}=50\%$. At the right side of this line, the heavy hole is mainly located inside the disk [Fig. 3(a)], and the system is type-I-like. At the left side of the 50% line, the heavy hole is predominantly located at the radial boundary outside of the disk [Fig. 3(b)], and the system is type-II-like.

From our previous work,[18,28] we know that when the hole is located at the radial boundary of the disk it will lead to the occurrence of hole angular momentum transitions as a function of a magnetic field applied parallel to the growth (z) direction. Such angular momentum transitions also occur for the exciton and are not found for type-I excitons.

IV. HEAVY-HOLE TO LIGHT-HOLE TRANSITION OF THE GROUND STATE

In the present approach, mixing of the valence bands is neglected and we thus solve two separate sets of coupled equations, namely, one for the heavy hole and one for the light hole. Next we will compare the energy of the light- and heavy-hole exciton in order to determine which one is the ground state. The results are summarized in Fig. 4, which shows a phase diagram of the heavy-to-light hole transition

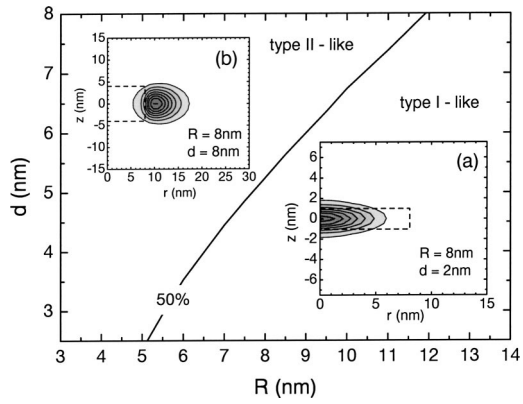

FIG. 3. Phase diagram for the probability for the heavy-hole to be located at the radial boundary of the disk, as a function of the disk radius and thickness. The curve denotes a probability of 50%. The insets show the heavy-hole wave functions for, respectively, a type-I-like system (a) and a type-II-like system (b).

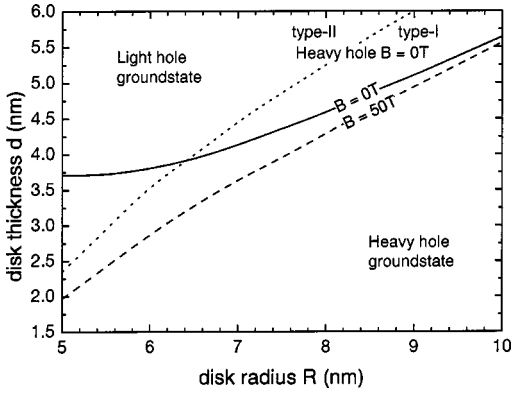

FIG. 4. Phase diagram indicating whether the heavy- or light-hole exciton is the ground state, as a function of the disk radius and thickness. The solid curve denotes the result for $B=0$, whereas the dashed curve gives the result for $B=50$ T. The dotted line indicates the 50% probability for the heavy-hole to be located at the radial boundary of the dot for $B=0$.

as a function of both R and d. We find that the light-hole exciton becomes the ground state for increasing thickness of the disk. The full curve in Fig. 4 shows the separation between the heavy- and light-hole exciton ground states in the absence of a magnetic field. The dotted curve is the result of Fig. 3, which separates the heavy-hole type-I and type-II ground state. Notice that the heavy-hole exciton is in the heavy-hole type-I region for $R>6.4$ nm. When the heavy hole is at the radial boundary outside the dot, the exciton energy is higher than that for the (type-II) light-hole exciton, except in a very narrow region of d values for $R<6.4$ nm.

The dashed curve shows the result for $B=50$ T. Thus a magnetic field lowers the light-hole ground state with respect to the heavy hole. This is made more clear in Fig. 5, where the evolution of the heavy- (full curve) and light-hole (dashed curve) exciton energies is shown as a function of magnetic field for a fixed disk size, i.e., $R=6.5$ nm and $d=3.5$ nm. The reason for this *magnetic-field induced heavy-to-light hole transition* can be found in the stronger effect of

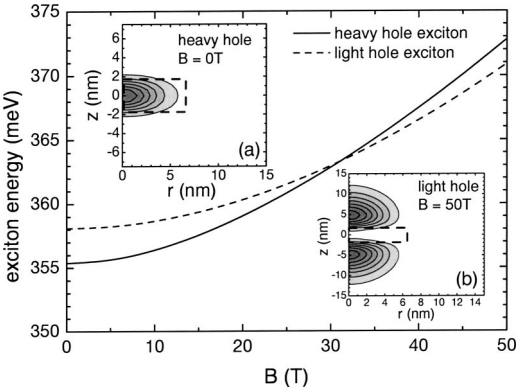

FIG. 5. The exciton energy as a function of the magnetic field for a disk with radius $R=6.5$ nm and thickness $d=3.5$ nm, both for the heavy-hole exciton (solid curve) and the light-hole exciton (dashed curve.) The insets show contour plots of the probability densities of, respectively, the heavy-hole at $B=0$ T (a) and the light-hole at $B=50$ T (b).

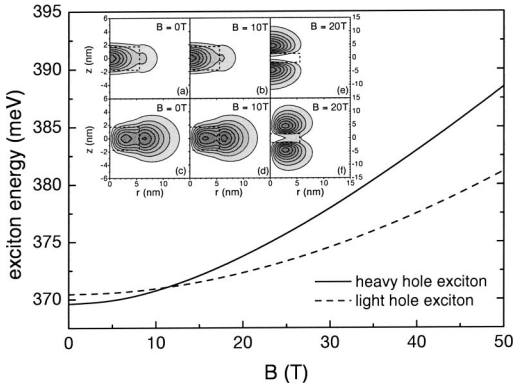

FIG. 6. The exciton energy as a function of the magnetic field for a disk with radius $R=5.5$ nm and thickness $d=3.5$ nm, both for the heavy-hole exciton (solid curve) and the light-hole exciton (dashed curve.) The insets show contour plots of, respectively, the probability densities and radial probability densities of the heavy-hole at $B=0$ T (a,c) and at $B=10$ T (b,d), and of the light-hole at $B=20$ T (e,f).

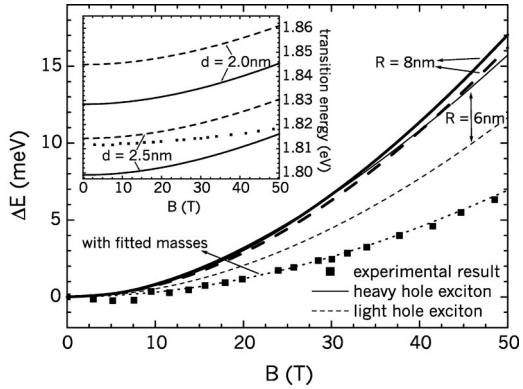

FIG. 7. The exciton diamagnetic shift as a function of the magnetic field, for a disk with thickness $d=2.5$ nm and for, respectively, $R=8$ nm (thick curves) and $R=6$ nm (thin curves). The solid curves indicate the heavy-hole exciton, whereas the dashed curves indicate the light-hole exciton. The dotted curve depicts the result with fitted masses. The squares denote the experimental result of Ref. 3. The inset depicts the exciton transition energy for a disk with radius $R=8$ nm and thickness $d=2$ nm and $d=2.5$ nm, as indicated in the plot. The solid curve denotes the heavy-hole exciton, whereas the dashed curve gives the result for the light-hole exciton.

the magnetic field on the heavy hole. This is due to a larger magnetic energy $\hbar\omega_{c,hh}=\hbar eB/m_{hh,\|}$, which is caused by a smaller in-plane heavy-hole mass, known as *mass reversal*.[30] The insets show, respectively, the heavy-hole wave function at $B=0$ T (a) and the light-hole wave function at $B=50$ T (b). Thus this heavy-light hole transition is accompanied with a spatial direct-to-indirect exciton transition.

It is also possible to have a magnetic-field induced heavy-to-light hole transition where both heavy- and light-hole exciton states are spatially indirect. This is shown in Fig. 6, where the evolution of the heavy- (full curve) and light- (dashed curve) hole excitons is depicted as a function of magnetic field for a disk with radius $R=5.5$ nm and thickness $d=3.5$ nm. In the insets are depicted both the probability density $|\Psi|^2$ (a,b,e) and the radial position probability density $r|\Psi|^2$ (c,d,f) for the hole in the exciton ground state, for different values of the magnetic field, as indicated. The heavy hole is shown in Figs. 6(a–d), where from the radial position probability density it follows that the system is indeed type II. An increasing magnetic field pushes the heavy-hole wave function more inside the disk, until it would eventually become type I. However, before this happens, the light-hole exciton becomes the ground state of the system, which is still type II, as shown in Figs. 6(e,f).

V. COMPARISON WITH EXPERIMENT

In order to compare our theoretical results with the magnetophotoluminescence experiments of Ref. 3, we have to calculate the exciton transition energy as a function of the magnetic field. The transition energy is defined as follows:

$$E_{trans}=E_{exciton}+E_g, \tag{8}$$

where E_g is the band-gap energy of the disk material and $E_{exciton}$ [Eq. (6)] contains the single-particle electron and hole energies and the Coulomb binding energy. Our theoretical results (curves) are compared with the experimental photoluminescence results (squares) from Hayne *et al.*[3] in the inset of Fig. 7. We show both the heavy- (full curve) and light- (dashed curve) hole exciton energies, for two values of the disk thickness: $d=2$ nm and $d=2.5$ nm, as indicated on the plot (the disk radius was taken $R=8$ nm for all curves). A change in the thickness almost uniformly shifts the curves up or down in energy, which is due to a corresponding change of the confinement energy (mostly of the electron). For these sets of disk parameters, the heavy-hole exciton is the ground state. But we find that the light-hole exciton for $d=2.5$ nm approaches most closely the experimental result for small B, while the heavy-hole results are closer for high B. By fine tuning the value of d, it is possible to fit the $B=0$ T heavy-hole transition energy to the experimental result. To show more clearly the magnetic-field dependence, we investigated the exciton diamagnetic shift, defined as

$$\Delta E=E_{trans}(B)-E_{trans}(B=0\ \text{T}). \tag{9}$$

The result is depicted in Fig. 7 for $d=2.5$ nm by the thick full (heavy hole) and dashed (light-hole) curves. Notice that the diamagnetic shift of the exciton is overestimated by more than a factor of 2 in the considered magnetic-field range.

In order to explain the discrepancy, we systematically investigated the influence of different disk and material parameters on the diamagnetic shift of the exciton. The results for $d=2$ nm are on top of the $d=2.5$ nm results. This is not too surprising because the disk thickness only minorly influences the in-plane motion. But a decrease of the disk radius will decrease the diamagnetic shift. However, even a substantial decrease to $R=6$ nm cannot explain the experimental results quantitatively, as shown in Fig. 7 by the thin curves, although the theoretical results are closer to the experimental results than for $R=8$ nm. We find that the light-hole exciton is most strongly affected and shows a smaller diamagnetic shift. However, the shift is still large for high fields, and thus

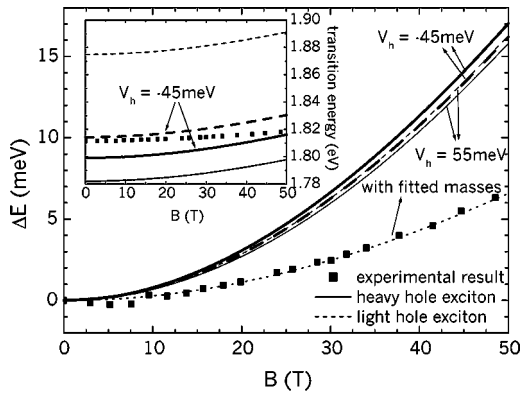

FIG. 8. The exciton diamagnetic shift as a function of the magnetic field for both a positive (thick curves) and a negative (thin curves) unstrained valence-band offset. The results for the heavy- and light-hole excitons are given by, respectively, the solid and dashed curves, while the squares indicate the experimental result of Ref. 3. The dotted curve denotes the results with fitted masses. Inset: The exciton transition energy as a function of the magnetic field. The same convention for the curves is used as in the main figure.

cannot be the main reason for the discrepancy. But from the phase diagram (Fig. 4), we know that the heavy-hole exciton is still the ground state and its diamagnetic shift decreased only by 7.7%. It would not be realistic to further decrease the disk radius, as measurements found a disk diameter ≈ 16 nm.

Next, the influence of the masses was investigated. In order to obtain a smaller diamagnetic shift, an increase of the masses is needed: the higher the mass, the stronger the particles are bound in the disk, and the smaller will be the influence of the magnetic field, i.e., the diamagnetic shift is inversely proportional to the exciton mass. For the electron, we increased the mass with a factor of 2, namely, $m_e^*(\mathrm{InP}) = 0.15m_0$. As the magnetic field acts mainly on the radial direction, a change of the in-plane mass ($m_\parallel$) will have the largest effect on the diamagnetic shift. We will, therefore, only vary this in-plane mass for the holes. Furthermore, we found that the heavy-hole is located in the disk, whereas the light hole is located in the barrier material. For the heavy-hole exciton we thus vary only the in-plane mass *in the disk*, while for the light-hole exciton we vary only the in-plane mass *in the barrier*. The results are shown by the dotted curve in Fig. 7. An excellent fit to the experimental diamagnetic shift with the heavy-hole exciton could be found (disk radius $R=8$ nm and thickness $d=2.5$ nm) for $m_{hh,\parallel} = 0.5m_0$, whereas for the light-hole, we found a good fit for $m_{lh,\parallel}=1.50m_0$.

The assumption of a negative band offset was questioned in Ref. 29 where a positive unstrained valence-band (VB) offset of 55 meV was found theoretically. The result for the transition energy with a positive unstrained hole band offset of $V_h=55$ meV is shown in the inset of Fig. 8, where we find that the heavy-hole now more closely approximates the experimental result, although the quantitative agreement is less good than that for a negative unstrained offset. Notice also the large difference between the results for heavy and light-holes. The reason is that the heavy-hole is now much stronger confined inside the disk. The corresponding diamagnetic shift is shown in Fig. 8 for $R=8$ nm and $d=2.5$ nm, where the results for the negative offset are shown by the thick curves, whereas the results for the positive offset are shown by the thin curves. We notice that the heavy-hole is more strongly affected by the reversed offset: the diamagnetic shift at $B=50$ T has decreased by ~ 5 meV. We attribute this to the stronger confinement of the heavy-hole inside the disk: as the hole will already be confined in the unstrained case, strain will only enhance this effect for the heavy-hole. Furthermore, a stronger potential confinement decreases the effect of the magnetic field on the particle. The light-hole, on the contrary, is only slightly affected by the altered band offset. Although the height of the potential barrier for the light hole has decreased, it is still appreciable, and will not have a drastic influence on the magnetic-field behavior of the light-hole. However, the qualitative discrepancy still exists in Fig. 8, which thus cannot be explained by the reversed band offset. Also for the case of the positive unstrained VB offset, we investigated the influence of the masses. Again we took a fixed electron mass in the dot of $m_e^*=0.15m_0$, both for the heavy-hole exciton and for the light-hole exciton. Furthermore, following the same reasoning as above, we only fitted the in-plane heavy- and light-hole masses. We found an excellent fit to the experimental results for $m_{hh,\parallel}=0.5m_0$ and $m_{lh,\parallel}=3.0m_0$ for, respectively, the heavy- and the light-hole exciton, which is shown in Fig. 8 by the dotted curve. Notice that in this case, we need a light-hole effective mass which is two times larger than that in the case of a negative unstrained offset. We attribute this to the fact that the light-hole is more weakly bound, and that thus a higher mass is needed to obtain a smaller diamagnetic shift.

From the above results, we can conclude that a change of the disk parameters (i.e., radius and/or thickness) is not the main origin of the discrepancy between theory and experiment. Furthermore, we find that taking a positive unstrained valence-band offset has only a minor influence to our theoretical results. However, both for the positive and for the negative unstrained offset, a change of the electron mass and of the in-plane hole masses could change drastically the diamagnetic shift, and a good fit to the experimental result could be obtained. Effects due to disorder may have an appreciable effect on the masses and are expected to increase them. But on the other hand, the use of the effective-mass approximation is questionable in such a situation.

VI. CONCLUSIONS

We have investigated theoretically the properties of an exciton in a strained self-assembled quantum dot. The dot was modeled by a disk and strain fields were taken into account using the isotropic elasticity model. The exciton energy and wave function were obtained by means of a mean-field theory using the Hartree approximation.

Investigation of the effect of strain on the confinement potentials tells us that, starting from a negative (type-II) unstrained valence-band offset, the confinement potential for

the heavy-hole is reversed (i.e., becomes type I), while for the light-hole the system becomes even stronger type II. However, with increasing disk thickness, the heavy-hole potential inside the disk was found to decrease strongly with respect to a potential maximum at the radial boundary outside the disk. For a certain disk thickness, it becomes thus preferential for the heavy-hole to move towards the radial boundary, into the barrier material, making the system also type II. A consequence of this behavior is the occurrence of angular momentum transitions for the heavy-hole when a magnetic field is applied.

A phase diagram was constructed as a function of the disk radius and thickness, indicating whether the heavy-hole exciton or the light-hole exciton forms the ground state of the system. This was done both for $B=0$ T and $B=50$ T. The magnetic field was found to be able to induce a heavy-to-light-hole transition. This magnetic-field induced transition was attributed to the heavy-hole mass, which has a smaller in-plane mass than the corresponding light-hole mass.

Finally, both the transition energy and the energy of the diamagnetic shift were calculated as a function of the magnetic field, and compared with experimental results by Hayne *et al.*[3,4] An appreciable discrepancy was found for the diamagnetic shift, and the origin of this discrepancy was investigated. We considered a smaller disk radius and found that this slightly decreases the difference between theory and experiment. Next, the masses were strongly increased, and we found that we can fit both the heavy- and the light-hole exciton energies to the experimental result. Furthermore, instead of taking a negative unstrained valence-band offset, we investigated the effect of starting with a positive unstrained offset. We found that this gives only a minor change in the theoretical results, and that again an increase of the masses is needed to obtain a good fit.

As far as the experimental result is concerned, we may conclude that from the diamagnetic shift, we find that the most plausible explanation for the small shift is an increase of the electron mass by a factor of 2, and as a consequence its value is closer to the $Ga_xIn_{1-x}P$ mass, and an increase of the in-plane heavy-hole mass such that its value is close to its perpendicular mass. Such increases in electron and hole masses are not unrealistic for a disordered quantum dot system. Thus the exciton observed by Hayne *et al.*[3] is most probably a type-I heavy-hole exciton in a strongly disordered quantum dot. In order to explain the experimental results in terms of a light-hole exciton, we have to increase the light-hole in-plane mass with approximately a factor of 10, which is rather unrealistic. Furthermore, it is the heavy-hole exciton which is the ground state of the system for the experimental value of the sizes of the quantum dot.

ACKNOWLEDGMENTS

K.L.J. was supported by the ''Instituut voor de aanmoediging van Innovatie door Wetenschap en Technologie in Vlaanderen'' (IWT-Vl) and B.P. was supported by Flemish Science Foundation (FWO-Vl). Part of this work was supported by the FWO-Vl, The Belgian Interuniversity Attraction Poles (IUAP), the Flemish Concerted Action (GOA) Program, the University of Antwerp (VIS) and the European Commission GROWTH program NANOMAT project, Contract No. G5RD-CT-2001-00545. We acknowledge interesting discussions with M. Tadić, M. Hayne, A. Zunger, A. Matulis, and J. Davies.

*Electronic address: karen.janssens@ua.ac.be

†Electronic address: bart.partoens@ua.ac.be

‡Electronic address: francois.peeters@ua.ac.be

[1] For a review, see, e.g., D. Bimberg, M. Grundmann, and N. N. Ledentsov, in *Quantum Dot Heterostructures* (Wiley, Chichester, 1999).

[2] Y. Arakawa and H. Sakaki, Appl. Phys. Lett. **40**, 939 (1982).

[3] M. Hayne, R. Provoost, M.K. Zundel, Y.M. Manz, K. Eberl, and V.V. Moshchalkov, Phys. Rev. B **62**, 10 324 (2000).

[4] M. Hayne, J. Maes, V.V. Moshchalkov, Y.M. Manz, O.G. Schmidt, and K. Eberl, Appl. Phys. Lett. **79**, 45 (2001).

[5] L. Müller-Kirsch, R. Heitz, A. Schliwa, O. Stier, D. Bimberg, H. Kirmse, and W. Neumann, Appl. Phys. Lett. **78**, 1418 (2001).

[6] R. Heitz, N.N. Ledentsov, D. Bimberg, M.V. Maximov, A.Yu. Egorov, V.M. Ustinov, A.E. Zhukov, Zh.I. Alferov, G.E. Cirlin, I.P. Shoshnikov, N.D. Zakharov, P. Werner, and U. Gösele, Appl. Phys. Lett. **74**, 1701 (1999).

[7] A. Polimeni, S.T. Stoddart, M. Henini, L. Eaves, P.C. Main, K. Uchida, R.K. Hayden, and N. Miura, Physica E (Amsterdam) **2**, 662 (1998).

[8] L.R. Wilson, D.J. Mowbray, M.S. Skolnick, M. Morifuji, M.J. Steer, I.A. Larkin, and M. Hopkinson, Phys. Rev. B **57**, R2073 (1998).

[9] O. Stier, M. Grundmann, and D. Bimberg, Phys. Rev. B **59**, 5688 (1999).

[10] M. Brasken, M. Lindberg, D. Sundholm, and J. Olsen, Phys. Rev. B **61**, 7652 (2000).

[11] M. Bayer, A. Schmidt, A. Forchel, F. Faller, T.L. Reinecke, P.A. Knipp, A.A. Dremin, and V.D. Kulakovskii, Phys. Rev. Lett. **74**, 3439 (1995).

[12] J. Song and S.E. Ulloa, Phys. Rev. B **52**, 9015 (1995).

[13] K.L. Janssens, F.M. Peeters, and V.A. Schweigert, Phys. Rev. B **63**, 205311 (2001).

[14] C. Pryor, M.-E. Pistol, and L. Samuelson, Phys. Rev. B **56**, 10 404 (1997).

[15] M. Tadić, F.M. Peeters, and K.L. Janssens, Phys. Rev. B **65**, 165333 (2002).

[16] Ph. Lelong, K. Suzuki, G. Bastard, H. Sakaki, and Y. Arakawa, Physica E (Amsterdam) **7**, 393 (2000).

[17] A.B. Kalameitsev, V.M. Kovalev, and A.O. Govorov, JETP Lett. **68**, 669 (1998).

[18] K.L. Janssens, B. Partoens, and F.M. Peeters, Phys. Rev. B **65**, 233301 (2002).

[19] K.L. Janssens, B. Partoens, and F.M. Peeters, Phys. Rev. B **66**, 075314 (2002).

[20] A.J. Williamson, L.W. Wang, and A. Zunger, Phys. Rev. B **62**, 12 963 (2000).

[21] M. Tadić, F.M. Peeters, K.L. Janssens, M. Korkusiński, and P. Hawrylak, J. Appl. Phys. **92**, 5819 (2002).

[22] C. Pryor, J. Kim, L.W. Wang, A.J. Williamson, and A. Zunger, J. Appl. Phys. **83**, 2548 (1998).

[23] J.R. Downes, D.A. Faux, and E.P. O'Reilly, J. Appl. Phys. **81**, 6700 (1997).
[24] J.D. Eshelby, Proc. R. Soc. London, Ser. A **241**, 376 (1957).
[25] J.H. Davies, J. Appl. Phys. **84**, 1358 (1998).
[26] M. Bayer, A. Schmidt, A. Forchel, A. Faller, T.L. Reinecke, P.A. Knipp, A.A. Dremin, and V.D. Kulakovskii, Phys. Rev. Lett. **74**, 3439 (1995); L. Jacak, P. Hawrylak, and A. Wójs, *Quantum Dots* (Springer-Verlag, Berlin, 1998), p. 25.
[27] O. Stier, *Electronic and Optical Properties of Quantum Dots and Wires* (Wissenschaft und Technik Verlag, Berlin, 2001).
[28] K.L. Janssens, B. Partoens, and F.M. Peeters, Phys. Rev. B **64**, 155324 (2001).
[29] S.-H. Wei and A. Zunger, Appl. Phys. Lett. **72**, 2011 (1998).
[30] P.Y. Yu and M. Cardona, *Fundamentals of Semiconductors: Physics and Material Properties* (Springer-Verlag, Berlin, 2001), p. 485.